Statistical Modeling of Asynchronous Impulsive Noise in Powerline Communication Networks

Marcel Nassar, Kapil Gulati, Yousof Mortazavi and Brian L. Evans
Department of Electrical and Computer Engineering
Wireless Networking and Communications Group
The University of Texas at Austin, Austin, Texas 78712 USA
Email: {nassar.marcel, ymortazavi}@mail.utexas.edu, {gulati, bevans}@ece.utexas.edu

***Abstract*—Powerline distribution networks are increasingly being employed to support smart grid communication infrastructure and in-home LAN connectivity. However, their primary function of power distribution results in a hostile environment for communication systems. In particular, asynchronous impulsive noise, with levels as high as 50 dB above thermal noise, causes significant degradation in communication performance. Much of the prior work uses limited empirical measurements to propose a statistical model for instantaneous statistics of asynchronous noise. In this paper, we (i) derive a canonical statistical-physical model of the instantaneous statistics of asynchronous noise based on the physical properties of the PLC network, and (ii) validate the distribution using simulated and measured PLC noise data. The results of this paper can be used to analyze, simulate, and mitigate the effect of the asynchronous noise on PLC systems.**

I. Introduction

Powerline networks are increasingly employed for communication purposes. These purposes vary from Internet connectivity inside the house to supporting smart grid applications such as automatic meter reading, device-specific billing and smart energy management. These powerline communication networks (PLC), initially designed for power transfer, result in a hostile environment for communication systems. Reflections and temporal variations in the PLC channel and correlated impulsive noise are the two main impairments for reliable communication [1]. This paper focuses on noise statistics, and refers readers interested in channel modeling to [1], [2], [3], [4], [5]. The non-Gaussian noise in PLC networks can be categorized into three main categories: generalized background noise, periodic impulsive noise, and asynchronous impulsive noise [6]. The first type has an exponentially decaying power spectral density superimposed with narrowband interference, while the second consists of broadband impulses occurring periodically. On the other hand, the asynchronous impulsive noise consists of random impulses of varying durations. It is mainly caused by switching transients of various appliances and devices in individual homes and businesses present on the network [1], [6]. Additional interference can also be picked up by the PLC network acting as an antenna for wireless in-band and aliased signals [1]. This impulsive noise, with levels as much as 50 dB above thermal noise, is considered the main cause of errors in PLC communications [1].

This work was supported by the Global Research Collaboration Program of the Semiconductor Research Corporation under Task Id 1836.063.

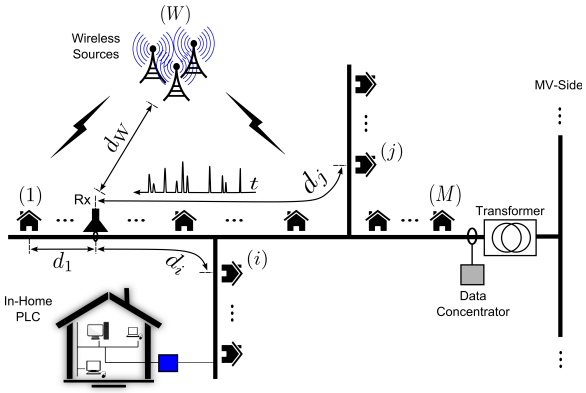

Fig. 1. A system model for a low-voltage powerline communications network and an in-home PLC LAN with interference sources. Each interference source can be either on the powerline or from an external wireless source. Each interferer emits asynchronous impulsive noise at a distance d_m from the receiver for $m = 1, \ldots, M$.

Frequency domain empirical studies fit the spectrally shaped background noise to various spectral models [7], [8]. Likewise, time domain properties of the asynchronous impulsive noise, such as impulse inter-arrival times, impulse durations, and instantaneous statistics, have been experimentally investigated in [3], [6], [8], [9]. We refer the reader to [3] and [6] for modeling the impulse inter-arrival times and impulse durations.

In this paper, we focus on the instantaneous amplitude statistics of the asynchronous impulsive noise which are important properties for communication system performance and simulation [10], [11], [12]. Prior work fits the noise data to different statistical models such as Middleton's Class A [10], Nakagami-m [11], and Rayleigh [9] distributions empirically without considering the underlying physical models of interference generation. Recent work in [13] supports the Gaussian mixture and Middleton noise models by filtering the interference through a PLC channel in a Monte Carlo simulation and studying the resulting statistics of the simulated noise. As a follow-up to previous work, we derive an analytical statistical-physical model of the first-order distribution of the asynchronous impulsive noise in PLC networks based on physical models of the PLC channel and the generated interference. Temporal and higher order statistics are left for future work. On top of that, we validate our models using

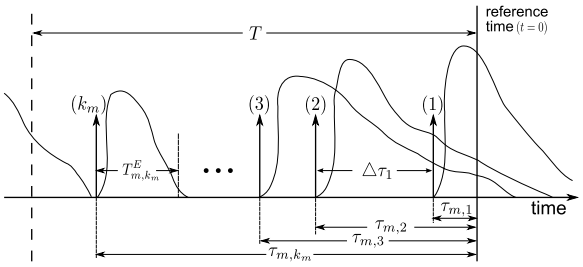

Fig. 2. Superposition of impulses generated by source m: vertical arrows are illustrations indicating arrivals, k_m is the number of arrivals within time duration T, and $t = 0$ is the reference time.

Monte-Carlo simulations and experimental data collected on a PLC network.

II. System Model

We consider a power-distribution or an indoor PLC network in which a randomly located receiver receives a signal of interest in the presence of interfering signals. A typical system model for a low-voltage PLC network is given in Fig. 1. In this model, there are M interferers that are a combination of various homes connected to a transformer and some wireless sources such as AM transmissions. The PLC environment is very dynamic and can exhibit different characteristics on hourly basis, such as variations in load impedances during the day period [1], [6], [14]. However, this paper focuses on deriving instantaneous impulse statistics as observed by a communication system. As a result, we ignore the large scale variations in the environment, and assume it to be stationary on the desired time scale. The interference experienced by a receiver at a reference time $t = 0$ due to emissions that arrived within a time interval of duration T from the reference time is given by

$$\mathbf{I}(T) = \sum_{m=1}^{M} \mathbf{I}_m(T) \tag{1}$$

where $\mathbf{I}_m(T)$ is the interference resulting from interference source m. Consequently, the interference due to all emissions that arrived in the past until time t is given by

$$\mathbf{\Psi} = \lim_{T\to\infty} \mathbf{I}(T). \tag{2}$$

Although taking $T \to \infty$ might contradict the stationarity assumption mentioned earlier, we will show that this is not the case and that it holds for the desired time scale as well. The objective is to find the first-order statistics of this total interference by calculating the characteristic function of $\mathbf{I}_m(T)$ for each interferer m. Toward this end, we focus on finding appropriate statistical models for the impulsive emissions based on experimental studies found in the literature (typically up to 20MHz).

A. Interference Emissions Modeling

Fig. 2 shows the superposition of impulsive emissions due to source m. Each impulse i is made up of two parameters: an arrival time relative to the reference time denoted by $\boldsymbol{\tau}_{m,i}$ (indicated by an arrow) and an impulse duration denoted by $\mathbf{T}^E_{m,i}$. The dynamics of the emissions are captured by the inter-arrival times between impulses denoted by $\{\triangle\boldsymbol{\tau}_i : i \in \mathbb{N}\}$. Various experimental studies investigated the temporal properties of asynchronous impulsive emissions in PLC networks [3], [6], [8], [9]. In particular, measurements done in [3] and [6] showed that the inter-arrival time between two consecutive impulses fits an exponential distribution; i.e., the inter-arrival time between impulse i and impulse $i+1$ has the following distribution

$$\triangle\boldsymbol{\tau}_{m,i} \sim \text{Exp}(\lambda_m)$$

where λ_m is the emission *rate* of source m. Since two impulses arriving at the same time are indistinguishable (they add up constructively), the process $\mathbf{\Lambda}_m = \{\boldsymbol{\tau}_{m,i} : i \in \mathbb{N}\}$ representing the impulse arrival times for source m is a counting process with jumps of size one. This combined with the exponential inter-arrival times, makes it a time Poisson point process with *rate* λ_m. As a result, the interference emissions in our model are characterized by a set of time Poisson point processes $\{\mathbf{\Lambda}_i(\lambda_i) : 1 \le i \le M\}$ corresponding to each interferer in Fig. 1. This modeling can be generalized to indoor PLC networks where the interference sources are individual appliances [3]. On the other hand, the statistics of the impulse duration $\mathbf{T}^E_{m,i}$ have been studied in [6], [8]. It was found that a typical impulse has a duration ranging from about 10μs to $1m$s with a distribution that is loosely exponential and a typical value of hundreds of μs [6]. The exact distribution of the impulse duration is not important since the derivation in this paper depends only on its first moment $\mathbb{E}\{\mathbf{T}^E_{m,i}\}$.

B. Interference Channel Modeling

The PLC channel properties have been studied extensively in [2], [4], [5]. In [4], the PLC channel was fitted to a time-domain pulse model. On the other hand, [2] and [5] exploit the physical properties of the transmission line. The two-port network model presented in [2], represents each component of the PLC network, such as a cable or a transformer, by its equivalent two-port network description (ABCD or S-parameters). Then, transmission line (TL) theory is used to compute the equivalent channels and reflection impedances. On the other hand, the echo model, presented in [5], is simplified representation of the channel frequency response inspired by TL theory. The echo model describes the channel by the following equation

$$\mathbf{H}(f) = \sum_{j=1}^{N} \mathbf{g}_j e^{-\alpha(f)d_j} e^{-j2\pi f d_j/\nu} \tag{3}$$

where N is the number of paths, $\mathbf{g}_j$ is a random variable representing the reflection coefficient of each propagation path that depends on the observed load impedance, $\alpha(f)$ is the attenuation constant of the cables used, d_j is the length of each reflection path needs to travel, and ν is signal propagation speed through the wire. The impulse response of this channel has a delay spread τ_h between 1μs to around 4μs [4], [5].

The effect of this channel on an impulse i due to source m can be inferred by comparing the typical values of $\mathbf{T}_{m,i}^{E}$, the impulse durations presented in Section II-A, to the channel delay spread τ_h given above. Since $\mathbf{T}_{m,i}^{E} \gg \tau_h$, the response of channel to the impulsive emission will have only one resolvable component and the channel will be a flat fading channel (the signal's propagation delay is much smaller than the impulse duration). A similar conclusion can be reached by looking at the channel's frequency response given in [4] and [5]. For an impulsive emission bandwidth between 1kHz and 100kHz corresponding to the aforementioned $\mathbf{T}_{m,i}^{E}$, the channel response is relatively flat. As a result, the discrete baseband equivalent channel of (3) is given by

$$\mathbf{h}\left[n\right] = \mathbf{h}e^{j\theta}e^{-\alpha_0 d}\delta\left[n\right] \tag{4}$$

where $\mathbf{h}$ is a random amplitude, $\boldsymbol{\theta}$ is a random phase uniformly distributed on $[0, 2\pi]$ under the uncorrelated fading assumption, $e^{-\alpha_0 d}$ is the path attenuation, d is the distance between the interferer and the receiver, and $\alpha_0 = \alpha\left(f_0\right)$ for some f_0 in the frequency band being considered (flat fading). Even if the channel exhibits frequency selectivity, the resulting multipath of the interference can be lumped together into one longer impulse with a different amplitude distribution. The derivation in this paper depends only on the second order moment of the channel amplitude and thus can be applied to any channel distributions. For a wireless interferer, we assume a Rayleigh flat fading channel with pathloss proportional to $d^{-\gamma/2}$, where d is the distance of the source and γ is the pathloss exponent [15].

III. Statistical Modeling of $\mathbf{I}_m\left(T\right)$

Fig. 2 shows a typical realization of impulse emissions within a window of duration T resulting from interference source m. The resulting interference at the receiver at a reference time $t = 0$, $\mathbf{I}_m\left(T\right)$, can be represented as

$$\mathbf{I}_m\left(T\right) = \gamma\left(d_m\right)\sum_{i=1}^{\mathbf{k}_m}\mathbf{h}_{m,i}e^{j\boldsymbol{\theta}_{m,i}}\mathbf{X}_{m,i} \tag{5}$$

where $\mathbf{k}_m$ is the number of impulses that arrived within a window of duration T, $\mathbf{h}_{m,i}e^{j\boldsymbol{\theta}_{m,i}}$ is the flat channel gain (based on (4)) between the interference source m and the receiver as seen by impulse i, and $\gamma\left(d_m\right)$ is the path attenuation. From Section II-B, the channel attenuation can be expressed as

$$\gamma\left(d_m\right) = \begin{cases} d_m^{-\eta/2} & \text{if } m \text{ is a wireless source} \\ e^{-\alpha_0 d_m} & \text{if } m \text{ is a wired source} \end{cases} \tag{6}$$

where d_m is the distance between the source and the receiver. On the other hand, $\mathbf{X}_{m,i}$ is the random emission due to the duration of impulse i and can be represented as

$$\mathbf{X}_{m,i} = \mathbf{B}_{m,i}e^{j\boldsymbol{\phi}_{m,i}}\mathbf{1}\left(\boldsymbol{\tau}_{m,i} \le \mathbf{T}_{m,i}^{E}\right) \tag{7}$$

where $\mathbf{1}\left(\cdot\right)$ is the indicator function, and $\mathbf{B}_i e^{j\boldsymbol{\phi}_i}$ represents the result of narrowband filtering of interference emissions performed at the receiver. The condition inside of the indicator function guarantees that the emission corresponding to impulse i is still active at the reference time $t = 0$ (See Fig. 2). For example, in Fig. 2 impulse k_m no longer has an effect at $t = 0$ while impulse 1 is still active as reflected in the indicator function's condition. $\mathbf{B}_i$ is an *i.i.d.* envelope and $\boldsymbol{\phi}_i$ is a random phase uniformly distributed on $[0, 2\pi]$. This representation is valid as long as $\mathbf{T}_{m,i}^{E} \gg \frac{1}{\triangle f_R}$ where $\triangle f_R$ is the receiver bandwidth [16]. This is the case for the values of $\mathbf{T}_{m,i}^{E}$ mentioned in Section II-A, especially for broadband PLC ($\triangle f_R \approx$ 1MHz). Expanding $\mathbf{I}_m\left(T\right)$ into its complex form, we obtain

$$\begin{aligned}\mathbf{I}_m\left(T\right) = &\sum_{i=1}^{\mathbf{k}_m}\mathbf{h}_{m,i}\mathbf{B}_{m,i}\mathbf{1}\left(\boldsymbol{\tau}_{m,i} \le \mathbf{T}_{m,i}^{E}\right) \\ &\times\left[\cos\left(\boldsymbol{\phi}_{m,i} + \boldsymbol{\theta}_{m,i}\right) + j\sin\left(\boldsymbol{\phi}_{m,i} + \boldsymbol{\theta}_{m,i}\right)\right].\end{aligned} \tag{8}$$

From (8), the joint characteristic function of the in-phase and quadrature-phase components of $\mathbf{I}_m\left(T\right) = \mathbf{I}_m^{(I)}\left(T\right) + j\mathbf{I}_m^{(Q)}\left(T\right)$, with implicit dependence on T, is given by

$$\begin{aligned}\Phi_{\mathbf{I}_m}\left(\omega\right) &= \mathbb{E}_{\mathbf{I}_m}\left\{e^{j\omega_I\mathbf{I}_m^{(I)} + j\omega_Q\mathbf{I}_m^{(Q)}}\right\} \\ &= \mathbb{E}\left\{e^{j\sum\limits_{i=1}^{\mathbf{k}_m}\mathbf{h}_{m,i}\mathbf{B}_{m,i}\mathbf{1}\left(\boldsymbol{\tau}_{m,i}\le\mathbf{T}_{m,i}^{E}\right)|\omega|\cos\left(\boldsymbol{\phi}_{m,i}+\boldsymbol{\theta}_{m,i}+\omega_\phi\right)}\right\}\end{aligned}$$

where $\mathbf{I}_m = \left[\mathbf{I}_m^{(I)}, \mathbf{I}_m^{(Q)}\right]^T$ and $\omega = \left[\omega_I, \omega_Q\right]^T$, $|\omega| = \sqrt{\omega_I^2 + \omega_Q^2}$, and $\omega_\phi = \tan^{-1}\left(\frac{\omega_Q}{\omega_I}\right)$. The expectation in the above equation is with respect to $\mathbf{k}_m$, $\left\{\mathbf{B}_{m,i}, \mathbf{h}_{m,i}, \boldsymbol{\tau}_{m,i}, \boldsymbol{\phi}_{m,i}, \boldsymbol{\theta}_{m,i}, \mathbf{T}_{m,i}^{E} : 1 \le i \le \mathbf{k}_m\right\}$. Taking the expectation over $\mathbf{k}_m$, we obtain

$$\begin{aligned}\Phi_{\mathbf{I}_m}\left(\omega\right) = &\sum_{k_m=0}^{\infty}\mathbb{P}\left(k_m \text{ arrivals in duration } T\right)\times \\ &\mathbb{E}\left\{e^{j\sum\limits_{i=1}^{k_m}\mathbf{h}_{m,i}\mathbf{B}_{m,i}\mathbf{1}\left(\boldsymbol{\tau}_{m,i}\le\mathbf{T}_{m,i}^{E}\right)|\omega|\cos\left(\boldsymbol{\phi}_{m,i}+\boldsymbol{\theta}_{m,i}+\omega_\phi\right)} \mid k_m\right\}\end{aligned} \tag{9}$$

Since $\boldsymbol{\Lambda}_m\left(\lambda_m\right)$ is a homogeneous Poisson time-point process, the number of impulse arrivals $\mathbf{k}_m$ in the window of duration T is Poisson distributed with distribution

$$\mathbf{k}_m \sim \text{Pois}\left(\lambda_m T\right).$$

Furthermore, given $\mathbf{k}_m$, the impulse arrival times $\left\{\boldsymbol{\tau}_{m,i} : 1 \le i \le \mathbf{k}_m\right\}$ are mutually independent and uniformly distributed on $[0, T]$; thus

$$\boldsymbol{\tau}_{m,i} \mid \mathbf{k}_m \sim \mathcal{U}\left(0, T\right) \text{ for } 1 \le i \le \mathbf{k}_m. \tag{10}$$

Assuming $\left\{\mathbf{B}_{m,i}, \mathbf{h}_{m,i}, \boldsymbol{\phi}_{m,i}, \boldsymbol{\theta}_{m,i}, \mathbf{T}_{m,i}^{E} \mid \mathbf{k}_m : 1 \le i \le k_m\right\}$ are all *i.i.d.* (i.e. statistically identical emissions for each impulse i), we can drop the index i and write (9) as

$$\begin{aligned}\Phi_{\mathbf{I}_m}\left(\omega\right) &= \sum_{k_m=0}^{\infty}\frac{e^{-\lambda_m T}\left(\lambda_m T\right)^{k_m}}{k_m!} \\ &\quad\times\left(\mathbb{E}\left\{e^{j|\omega|\mathbf{h}_m\mathbf{B}_m\mathbf{1}\left(\boldsymbol{\tau}_m\le\mathbf{T}_m^{E}\right)\cos\left(\boldsymbol{\phi}_m+\boldsymbol{\theta}_m+\omega_\phi\right)}\right\}\right)^{k_m} \\ &= e^{\lambda_m T\left(\mathbb{E}\left\{e^{j|\omega|\mathbf{h}_m\mathbf{B}_m\mathbf{1}\left(\boldsymbol{\tau}_m\le\mathbf{T}_m^{E}\right)\cos\left(\boldsymbol{\phi}_m+\boldsymbol{\theta}_m+\omega_\phi\right)}\right\}-1\right)}\end{aligned} \tag{11}$$

Denoting the expectation in (11) by $\psi_{\mathbf{I}_m}(\omega)$, we obtain

$$\begin{aligned}\psi_{\mathbf{I}_m}(\omega) &\triangleq \mathbb{E}\left\{e^{j|\omega|\mathbf{h}_m\mathbf{B}_m\mathbf{1}\left(\boldsymbol{\tau}_m\leq\mathbf{T}_m^E\right)\cos(\boldsymbol{\phi}_m+\boldsymbol{\theta}_m+\omega_\phi)}\right\}\\ &\overset{(a)}{=} \mathbb{E}\left\{\left(1-\frac{\mathbf{T}_m^E}{T}\right)e^0+\frac{\mathbf{T}_m^E}{T}e^{j|\omega|\mathbf{h}_m\mathbf{B}_m\cos(\boldsymbol{\phi}_m+\boldsymbol{\theta}_m+\omega_\phi)}\right\}\\ &\overset{(b)}{=} 1-\frac{\mu_m}{T}+\frac{\mu_m}{T}\mathbb{E}\left\{e^{j|\omega|\mathbf{h}_m\mathbf{B}_m\cos(\boldsymbol{\phi}_m+\boldsymbol{\theta}_m+\omega_\phi)}\right\} \qquad (12)\end{aligned}$$

where step (a) follows from taking the expectation over $\boldsymbol{\tau}_m$, and step (b) from taking the expectation over $\mathbf{T}_m^E$ with the notation $\mu_m = \mathbb{E}\{\mathbf{T}_m^E\}$. In step (a), we made the implicit assumption that $T > \mathbf{T}_m^E(\omega), \forall\omega \in \Omega$ where Ω is the probability space. This assumption is valid since in practice $\mathbf{T}_m^E$, the impulse duration, is bounded and follows a truncated distribution [6]. Further, (2) shows that we are interested in the limit as $T\to\infty$ which justifies our assumption. By using the identity

$$e^{ja\cos(\theta)} = \sum_{k=0}^{\infty} j^k\epsilon_k J_k(a)\cos(k\theta) \qquad (13)$$

where J_k is the Bessel function of the k-th order, $\epsilon_0 = 1$ and $\epsilon_k = 2$ for $k\geq 1$, (12) can be written as

$$\begin{aligned}\psi_{\mathbf{I}_m}(\omega) = 1-\frac{\mu_m}{T}+\frac{\mu_m}{T}\mathbb{E}\Bigg\{&\sum_{k=0}^{\infty} j^k\epsilon_k J_k(|\omega|\,\mathbf{h}_m\mathbf{B}_m)\\ &\times\cos\left(k\left(\boldsymbol{\phi}_m+\boldsymbol{\theta}_m+\omega_\phi\right)\right)\Bigg\}. \qquad (14)\end{aligned}$$

Since $\boldsymbol{\phi}_m$ and $\boldsymbol{\theta}_m$ are uniformly distributed on $[0,2\pi]$, $\mathbb{E}_{\phi_m,\theta_m}\{\cos(k(\boldsymbol{\phi}_m+\boldsymbol{\theta}_m+\omega_\phi))\} = 0$ for $k\geq 1$, and (14) reduces to

$$\psi_{\mathbf{I}_m}(\omega) = 1-\frac{\mu_m}{T}+\frac{\mu_m}{T}\mathbb{E}_{\mathbf{h}_m,\mathbf{B}_m}\{J_0(|\omega|\,\mathbf{h}_m\mathbf{B}_m)\}. \qquad (15)$$

An approximation for the expectation term in (15) is given by

$$\mathbb{E}_{\mathbf{h}_m,\mathbf{B}_m}\{J_0(|\omega|\,\mathbf{h}_m\mathbf{B}_m)\} = e^{\frac{-|\omega|\mathbb{E}\left\{\mathbf{h}_m^2\mathbf{B}_m^2\right\}}{4}}\left(1+\Theta\left(|\omega|^4\right)\right) \qquad (16)$$

where $\Theta\left(|\omega|^4\right)$ denotes a correction term with the lowest power of $|\omega|$ being four [16]. Fourier analysis shows that the behavior of the characteristic function in the neighborhood of zero governs the tail probabilities of the random variable. As a result, $\Theta\left(|w|^4\right)\ll 1$ for $|w|\to 0$, and can be ignored from (16) for modeling tail probabilities. For $\mathbf{h}_m\mathbf{B}_m$ Rayleigh distributed, $\Theta\left(|w|^4\right) = 0$ and the following result is exact. Substituting (16) into (15) and then into (11), we obtain

$$\begin{aligned}\Phi_{\mathbf{I}_m}(\omega) &= e^{\lambda_m\mu_m\left(-1+e^{\frac{-|w|^2\mathbb{E}\left\{\mathbf{h}_m^2\mathbf{B}_m^2\right\}}{4}}\right)}\\ &= e^{-\lambda_m\mu_m}\sum_{k=0}^{\infty}\frac{(\lambda_m\mu_m)^k}{k!}e^{\frac{-k|w|^2\mathbb{E}\left\{\mathbf{h}_m^2\mathbf{B}_m^2\right\}}{4}} \qquad (17)\end{aligned}$$

where the second step follows from the Taylor expansion of the exponential function. Two important observations can be made about (17): 1) there is no dependence on T, and (2) it is the characteristic function of a Middleton Class A distribution with parameters given by

$$A_m = \lambda_m\mu_m = \lambda_m\mathbb{E}\{\mathbf{T}_m^E\} \qquad (18)$$

$$\Omega_m = \frac{A_m\times\mathbb{E}\{\mathbf{h}_m^2\mathbf{B}_m^2\}}{2} = \frac{A_m\gamma(d_m)\,\mathbb{E}\{\mathbf{g}_m^2\mathbf{B}_m^2\}}{2} \qquad (19)$$

where A_m is the overlap index that indicates the amount of impulsiveness of the interference originating from source m, and Ω_m is its mean intensity. The independence of (17) from T is important for deriving the statistics of the total interference and is discussed in the following section.

IV. Statistical Modeling of the Total Interference $\boldsymbol{\Psi}$

The total interference as seen by the receiver is the superposition of impulses resulting from all available interference sources. Further, it should encompass the contribution of the impulse durations potentially spanning infinitely in the past. This is reflected in (2). However, as seen from (17), the statistics of the total interference $\boldsymbol{\Psi}$ depend only on the impulses that arrived within the maximum impulse duration which is finite. This has a simple intuitive explanation: any impulse that arrived before the maximum impulse duration would have died out by the reference time $t = 0$. On top of that, the maximum impulse duration is on the order of milliseconds (only 1% of total impulses exhibit a duration exceeding 1ms [6]). This duration is much lower than the rate of variation in the PLC enviroment characteristic which are on the order of hours and days [14]. This justifies the stationarity assumption mentioned in Section II.

Let $\xi = \max\left\{\mathbf{T}_m^E(\omega):\omega\in\Omega, 1\leq m\leq M\right\}$, then (2) can be expressed as

$$\boldsymbol{\Psi} = \lim_{T\to\infty}\mathbf{I}(T) = \mathbf{I}(\xi) = \sum_{m=1}^{M}\mathbf{I}_m(\xi). \qquad (20)$$

Assuming that impulses from different interference sources are independent and using the result from (17), we can express the characteristic function of the total interference as

$$\begin{aligned}\Phi_\Psi(\omega) = e^{-\sum_{m=1}^{M}\lambda_m\mu_m^E}&\sum_{k_1=0}^{\infty}\cdots\sum_{k_M=0}^{\infty}\prod_{m=0}^{M}\frac{\left(\mu_m^E\lambda_m\right)^{k_m}}{k_m!}\\ &\times e^{-|\omega|^2\sum_{m=1}^{M}k_m\gamma(d_m)\mathbb{E}\left\{\mathbf{g}_m^2\mathbf{B}_m^2\right\}/4}. \qquad (21)\end{aligned}$$

This is the characteristic function of a Gaussian mixture distribution. Truncating the each infinite summation into N terms, (21) can be simplified into the more familiar form

$$\Phi_\Psi(\omega) = \sum_{i=1}^{N^M}\pi_i e^{-|\omega|^2\sigma_i^2} \qquad (22)$$

where

$$\pi = \begin{bmatrix}\frac{\lambda_1^0 e^{-\mu_1\lambda_1}}{0!}\\ \vdots\\ \frac{\lambda_1^N e^{-\mu_1\lambda_1}}{N!}\end{bmatrix}\otimes\cdots\otimes\begin{bmatrix}\frac{\lambda_M^0 e^{-\mu_M\lambda_M}}{0!}\\ \vdots\\ \frac{\lambda_M^N e^{-\mu_M\lambda_M}}{N!}\end{bmatrix}$$

TABLE I

STATISTICAL-PHYSICAL MODELING OF ASYNCHRONOUS IMPULSIVE NOISE IN DIFFERENT PLC NETWORKS. FOR EACH INTERFERING SOURCE m, λ_m IS THE EMISSION RATE, μ_m IS THE MEAN, AND d_m IS THE DISTANCE TO THE RECEIVER. THERE ARE M INTERFERING SOURCES.

Scenario	Model
General PLC network $\{\lambda_m, \mu_m, d_m : 1 \leq m \leq M\}$	Gaussian Mixture π, σ^2 in (22)
One Dominant Interference Source λ, μ, d	Middleton's Class A $A = \lambda\mu, \Omega = \frac{A\gamma(d)\mathbb{E}\{\mathbf{h}^2\mathbf{B}^2\}}{2}$
Homogeneous PLC network $\lambda_m = \lambda, \mu_m = \mu, \gamma(d_m) = \gamma$ $\forall m \in \{1, \cdots, M\}$	Middleton's Class A $A = M\lambda\mu, \Omega = \frac{\lambda\mu\gamma\mathbb{E}\{\mathbf{h}^2\mathbf{B}^2\}}{2}$

and

$$\sigma^2 = \frac{1}{4}\begin{bmatrix} 0 \cdot \mathbb{E}\left\{\mathbf{h}_1^2\mathbf{B}_1^2\right\} \\ \vdots \\ N \cdot \mathbb{E}\left\{\mathbf{h}_1^2\mathbf{B}_1^2\right\} \end{bmatrix} \oplus \cdots \oplus \begin{bmatrix} 0 \cdot \mathbb{E}\left\{\mathbf{h}_M^2\mathbf{B}_M^2\right\} \\ \vdots \\ N \cdot \mathbb{E}\left\{\mathbf{h}_M^2\mathbf{B}_M^2\right\} \end{bmatrix}$$

where $\pi = \begin{bmatrix} \pi_1 & \cdots & \pi_{N^M} \end{bmatrix}$ and $\sigma^2 = \begin{bmatrix} \sigma_1^2 & \cdots & \sigma_{N^M}^2 \end{bmatrix}$. The operations $\otimes$ and $\oplus$ denote the Kronecker multiplication and sum respectively. These equations can be made arbitrary accurate by increasing N; however, 2 to 3 terms are usually sufficient in practice [17]. The amplitude distribution of the total interference can be deduced from (22) and written as

$$f_{|\Psi|}(\zeta) = \sum_{i=1}^{N^M} \pi_i e^{-|\omega|^2\sigma_i^2} \frac{\zeta}{\sigma_i^2} e^{-\zeta^2/\sigma_i^2}$$

which is a sum of Rayleigh distributions.

V. DISCUSSION

Eq. (21) and (22) describe the interference statistics under the general conditions given in Fig. 1. These equations can be further simplified by assuming more homogeneous environments with similar properties such as emission rates and channel and emission's amplitudes statistics. For example, environments with one dominant interference source will follow a Middleton Class A model with parameters given in (18) and (19). Environments with interference sources having similar rates, channel and emission statistics would also have a Middleton Class A statistics. To see this, assume that $\lambda_m = \lambda$, $\mu_m = \mu$, $\gamma(d_m) = \gamma$ and $\mathbb{E}\left\{\mathbf{g}_m^2\mathbf{B}_m^2\right\} = k \ \forall m \in 1, \cdots, M$. Substituting these values into (18) and (19) we get, for each interference source $m \in \{1, \cdots, M\}$,

$$A_m = \lambda\mu \qquad \Omega_m = \frac{\lambda\mu \times \gamma k}{2} \ . \tag{23}$$

Thus, the total interference $\mathbf{\Psi}$ is the sum of M independent Class A distributed random variables with parameters given by (23). Consequently, $\mathbf{\Psi}$ is also Class A distributed with the following parameters [17]

$$A_\Psi = MA_m \qquad \Omega_\Psi = \Omega_m \ . \tag{24}$$

The variance of the noise is also multiplied by M. The assumption that $\gamma(d_m)$ is independent of d_m is especially valid in lower frequency PLC networks (order of 100kHz) since for wired sources

$$\gamma(d_m) = e^{-\alpha(f_0)d_m} = e^{-\left(a_0 + a_1 f_0^k\right)d_m} \approx 1$$

where the last equality follows by substituting some measured values of the given parameters: $a_0 = 0$, $a_1 = 7.8 \times 10^{-10}$, $f_0 = 100$kHz, $k = 1$ and d_m having typical PLC network dimensions ($20m \leq d_m \leq 500m$) [5]. In this range the transmission line effects are negligible and lumped discrete models can be used. These cases are summarized in Table I.

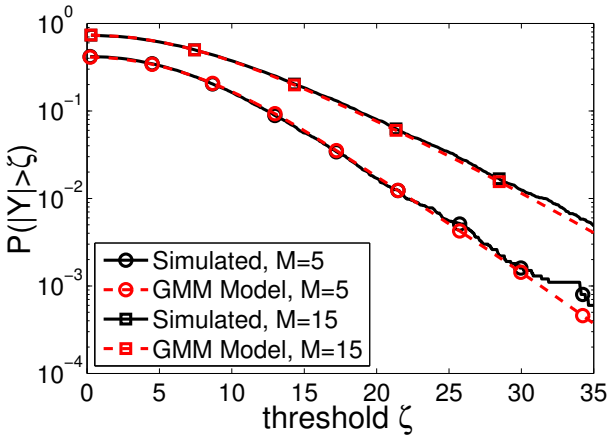

Fig. 3. For M different interfering sources, empirical tail probabilities from Monte-Carlo simulations and the predicted tail probabilities from the Gaussian mixture model given in (22) are shown. In both cases, the curves match exactly for a wide range of ζ values.

VI. SIMULATION AND EXPERIMENTAL RESULTS

We verify our derived models by using Monte-Carlo simulations of the system given in Fig. 1. In particular, for each interferer source m we choose a *rate* λ_m and distance d_m such that $\lambda_m \sim \mathcal{U}(\lambda_{\min}, \lambda_{\max})$ and $d_m \sim \mathcal{U}(d_{\min}, d_{\max})$. We choose $\lambda_{\min} = 50/\text{sec}$ and $\lambda_{\max} = 1000/\text{sec}$ based on empirical measurements [6], [1]. Also, we choose to simulate a medium-sized PLC network with $d_{\min} = 50$m, $d_{\max} = 500$m, and $\alpha_0 = 10^{-4}$ with the number of interference sources $M = 5, 15$. The mean impulse duration $\mathbb{E}\left\{\mathbf{T}_m^E\right\}$ was chosen to be 150μsec $\forall m$ [6]. The accuracy of the statistical models is established by comparing the empirical tail probabilities based on the Monte-Carlo simulated data and analytical tail probabilities predicted by our derived models. The tail probability characterizes the impulsiveness of a given distribution and is given by $\mathbb{P}(|Y| > y)$. The comparison between the two tail probabilities for the general cases where the number of interference sources is 5 and 15 is given in Fig. 3. The empirical tail probability curve and the model predicted tail probability curve are exact matches with little deviation at the higher amplitudes due to the limited number of data points generated in that range. Moreover, the curves corresponding to the case with 15 interference sources is higher than that of 5 sources because the variance (power) is higher for the former. On the other hand, Fig. 4 shows the tail probabilities for the

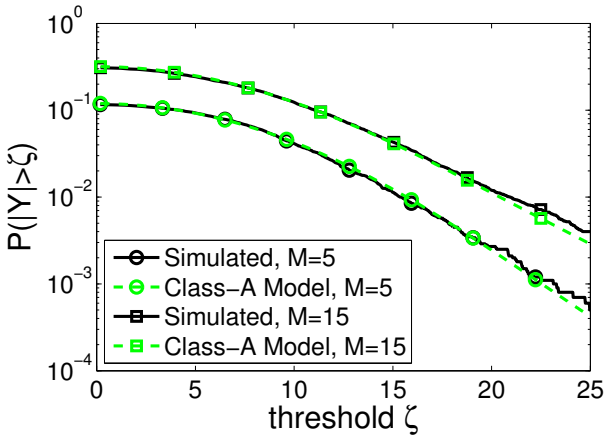

Fig. 4. For M homogeneous interfering sources with similar statistics, empirical tail probabilities from Monte-Carlo simulations and the predicted tail probabilities from the Middleton Class A model given in (24) are shown. In both cases, the curves match exactly for a wide range of ζ values.

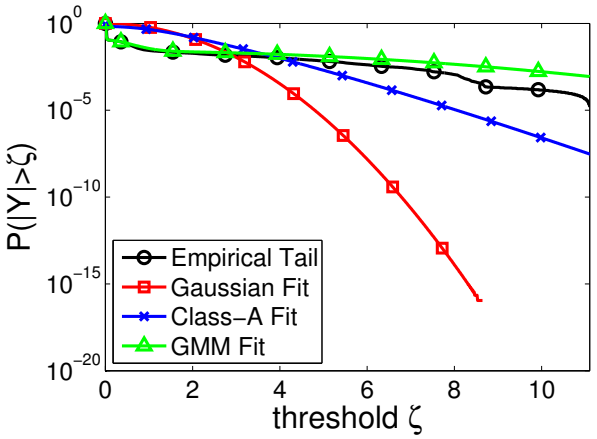

Fig. 5. Comparison of tail probabilities obtained from measured data samples and by the Gaussian distribution, Middleton Class A distribution, and Gaussian mixture model. The Gaussian mixture model provides the best fit among the derived models.

homogeneous network described in Section V. This network can be an appropriate approximation for low-frequency PLC networks and results in interference that is Middleton Class A distributed with parameters given in (24). Again, it can be seen that there is a good fit between the simulated data and the derived model.

In order to validate the above model, we captured real PLC network interference samples in an apartment building in Austin, TX. The noise was sampled in the $45-90$ kHz band at 1MSample/sec. We used the EM algorithm to fit the gathered data in chunks of 14 ms to the proposed models. The results, given by the tail probabilities, are shown in Fig. 5. The Gaussian mixture model provides the best fit in accordance with our derived model. The Class A model does not fit well in this particular case indicating that the interference sources had different emission properties. As expected, the Gaussian model provided the worst fit because it does not take into consideration the heavy tails of the interference distribution.

VII. Conclusion

This papers derives canonical statistical-physical models for the first order *pdfs* of the asynchronous impulsive noise present in general PLC networks. The derivation is based on the physical models of the PLC channel and the temporal models of the interarrival and duration of interference impulses. These models are then validated using simulated and experimental data. In conclusion, these models can be used to analyze, simulate and evaluate the performance of various PLC systems for different applications and study the properties and nature of asynchronous interference in PLC networks.

References

[1] H. Hrasnica, A. Haidine, and R. Lehnert, *Broadband Powerline Communications: Network Design*. Wiley, 2004.

[2] T. Banwell and S. Galli, "A new approach to the modeling of the transfer function of the power line channel," *Proc. Int. Symp. Power-Line Commun. and Appl.*, pp. 319–324, 2001.

[3] L. Tang, P. So, E. Gunawan, S. Chen, T. Lie, and Y. Guan, "Characterization of power distribution lines for high-speed data transmission," in *Proc. Int. Conf. on Power System Technology*, vol. 1, 2000, pp. 445–450.

[4] N. Gonzalez-Prelcic, C. Mosquera, N. Degara, and A. Currais, "A channel model for the galician low voltage mains network," *Proc. Int. Symp. Power-Line Commun. and Appl.*, pp. 365–370, 2001.

[5] M. Zimmermann and K. Dostert, "A multipath model for the powerline channel," *IEEE Trans. Commun.*, vol. 50, no. 4, pp. 553–559, 2002.

[6] ——, "Analysis and modeling of impulsive noise in broad-band powerline communications," *IEEE Trans. Electromagn. Compat.*, vol. 44, no. 1, pp. 249–258, 2002.

[7] O. Hooijen, "On the channel capacity of the residential power circuit used as a digital communications medium," *IEEE Commun. Lett.*, vol. 2, no. 10, pp. 267–268, 1998.

[8] J. Cortes, L. Diez, F. Canete, and J. Sanchez-Martinez, "Analysis of the indoor broadband power-line noise scenario," *IEEE Trans. Electromagn. Compat.*, vol. 52, no. 4, pp. 849–858, 2010.

[9] M. Chan and R. Donaldson, "Amplitude, width, and interarrival distributions for noise impulses on intrabuilding power line communication networks," *IEEE Trans. Electromagn. Compat.*, vol. 31, no. 3, pp. 320–323, 1989.

[10] D. Umehara, H. Yamaguchi, and Y. Morihiro, "Turbo decoding in impulsive noise environment," in *Proc. IEEE Global Telecommun. Conf.*, vol. 1, 2004, pp. 194–198.

[11] H. Meng, Y. Guan, and S. Chen, "Modeling and analysis of noise effects on broadband power-line communications," *IEEE Trans. Power Del.*, vol. 20, no. 2, pp. 630–637, 2005.

[12] N. Andreadou and F.-N. Pavlidou, "Modeling the noise on the OFDM power-line communications system," *IEEE Trans. Power Del.*, vol. 25, no. 1, pp. 150–157, 2010.

[13] L. Di Bert, P. Caldera, D. Schwingshackl, and A. Tonello, "On noise modeling for power line communications," in *Proc. Int. Symp. Power-Line Comm. and its Appl.*, 2011, pp. 283–288.

[14] M. Tanaka, "High frequency noise power spectrum, impedance and transmission loss of power line in Japan on intrabuilding power line communications," *IEEE Trans. Consum. Electron.*, vol. 34, no. 2, pp. 321–326, 1988.

[15] D. Tse and P. Viswanath, *Fundamentals of Wireless Communications*. Cambridge, 2005.

[16] D. Middleton, "Statistical-physical models of electromagnetic interference," *IEEE Trans. Electromagn. Compat.*, vol. 19, no. 3, pp. 106–127, 1977.

[17] Y. Matsumoto, K. Gotoh, and K. Wiklundh, "Band-limitation effect on statistical properties of class-A interference," in *IEEE Proc. Int. Symp. on Electromagn. Compat.*, 2008, pp. 1–5.